Mouse hepatitis virus nsp14 exoribonuclease activity is required for resistance to innate immunity

James Brett Case,[a,c] Yize Li,[d] Ruth Elliott,[d] Xiaotao Lu,[b,c] Kevin W. Graepel,[a,c] Nicole R. Sexton,[a,b,c] Everett Clinton Smith,[e] Susan R. Weiss,[d] and Mark R. Denison[a,b,c*]

Departments of Pathology, Microbiology, and Immunology[a] and Pediatrics[b] and Elizabeth B. Lamb Center for Pediatric Research,[c] Vanderbilt University Medical Center, Nashville, Tennessee, USA; Department of Microbiology,[d] Perelman School of Medicine, University of Pennsylvania, Philadelphia, Pennsylvania, USA; Department of Biology,[e] The University of the South, Sewanee, Tennessee, USA.

[*]**Corresponding author:** Mark R. Denison

E-mail: mark.denison@vanderbilt.edu

Running title: nsp14 ExoN activity is required for resistance to IFN

Keywords: coronavirus, MHV, exoribonuclease, ExoN, innate immunity, interferon

Word Count: (246 abstract; 123 importance)

ABSTRACT

Coronaviruses (CoV) are positive-sense RNA viruses that infect numerous mammalian and avian species and are capable of causing severe and lethal disease in humans. CoVs encode several innate immune antagonists that interact with the host innate immune response to facilitate efficient viral replication. CoV non-structural protein 14 (nsp14) encodes 3'-to-5' exoribonuclease activity (ExoN), which performs a proofreading function and is required for high-fidelity replication. Outside of the order *Nidovirales*, arenaviruses are the only RNA viruses that encode an ExoN, which functions to degrade dsRNA replication intermediates. In this study, we tested the hypothesis that CoV ExoN may also function to antagonize the innate immune response. We demonstrate that viruses lacking ExoN activity [ExoN(-)] are sensitive to cellular pretreatment with interferon beta (IFN-β) in a dose-dependent manner. In addition, ExoN(-) virus replication was attenuated in wild-type bone marrow-derived macrophages (BMMs) and partially restored in interferon alpha/beta receptor deficient (IFNAR-/-) BMMs. ExoN(-) virus replication did not result in IFN-β gene expression, and in the presence of an IFN-β-mediated antiviral state, ExoN(-) viral RNA levels were not substantially reduced relative to untreated. However, ExoN(-) virus generated from IFN-β pretreated cells had reduced specific infectivity and decreased relative fitness, suggesting that ExoN(-) virus generated during an antiviral state is less viable to establish a subsequent infection. Overall, our data suggest MHV ExoN activity is required for resistance to the innate immune response and antiviral mechanisms affecting the viral RNA sequence and/or an RNA modification act on viruses lacking ExoN activity.

IMPORTANCE

CoVs encode multiple antagonists that prevent or disrupt an efficient innate response. Additionally, no specific antiviral therapies or vaccines currently exist for human CoV infections. Therefore, the study of CoV innate immune antagonists is essential for understanding how CoVs overcome host defenses and to maximize potential therapeutic interventions. Here, we sought to determine the contributions of nsp14 ExoN activity in the induction of and resistance to the innate immune response. We show that viruses lacking nsp14-ExoN activity are more sensitive to restriction by exogenous IFN-β and that viruses produced in the presence of an antiviral state are less capable of establishing a subsequent viral infection. Our results support the hypothesis that MHV ExoN activity is required for resistance to the innate immune response.

INTRODUCTION

The innate immune response within a mammalian cell is the first line of defense against an invading pathogen. However, as obligate intracellular parasites, viruses have evolved numerous mechanisms to prevent and antagonize innate detection by host cells. Coronaviruses (CoVs), which are the largest known positive-sense, single-stranded RNA viruses, encode several type I interferon (IFN) antagonists. Many of these antagonists prevent the induction of IFN, while others mediate resistance to the effects of IFN (1-3). Upon secretion from a cell, IFNs bind to cell surface-expressed IFN-α/β receptors (IFNARs) in an autocrine and paracrine manner. Subsequently, an IFN signaling cascade utilizing the Janus kinase and signal transducer and activator of transcription pathway leads to the induction and expression of hundreds of interferon stimulated genes (ISGs) that act to limit or prevent viral replication and spread (4). However, during CoV infection, nonstructural protein (nsp) 1 antagonizes the innate immune response by degrading host mRNAs and suppressing IFN beta (IFN-β) expression (5, 6). The nsp3 of severe acute respiratory syndrome coronavirus (SARS-CoV) prevents IRF3 phosphorylation and NF-κB signaling (7). In addition, SARS-CoV nsp3 encodes deubiquitinating and deISGylating activities (3, 8). CoV viral RNA evades innate detection by pattern recognition receptors (PRRs) such as MDA5, and antiviral effectors, such as IFIT1, through formation of a 5’ cap-1 structure by encoding N7-methyltransferase and 2’O-methyltransferase activities within nsp14 and nsp16, respectively (9, 10). Murine hepatitis virus (MHV) and Middle East respiratory syndrome coronavirus (MERS-CoV) also encode 2’-5’ phosphodiesterases that degrade 2’-5’ oligoadenylates, which are key signaling molecules generated by oligoadenylate synthetase (OAS) in response to innate detection of dsRNA that subsequently activate RNase L (11). Most

89 recently, a CoV nsp15 endonuclease activity (EndoU) mutant virus was shown to have increased
90 dsRNA levels, suggesting that nsp15 EndoU reduces dsRNA levels during infection (12).
91 CoV nsp14 encodes 3'-to-5' exoribonuclease (ExoN) and N7-methyltransferase (N7-
92 MTase) activities (9, 13). CoV nsp14 N7-MTase activity is essential for efficient translation of
93 the viral genome and preventing innate detection (14). In addition, initial biochemical studies of
94 nsp14 ExoN activity demonstrated that ExoN has a preference for dsRNA and the capacity to
95 excise 3' end misincorporated nucleotides (13). Moreover, nsp14 ExoN activity is required for
96 high-fidelity replication. The CoV nsp14 ExoN is a member of the DE-D-Dh superfamily of
97 DNA and RNA exonucleases, so named for the three motifs of four active site residues (13).
98 *Betacoronaviruses* SARS-CoV and MHV expressing engineered, ExoN-inactivating
99 substitutions at active site residues in Motif I (DE→AA) [ExoN(-)] demonstrate increased
100 mutation frequencies and are profoundly sensitive to inhibition by RNA mutagens (15, 16).
101 Additionally, SARS-CoV ExoN(-) virus is attenuated *in vivo* (17). Interestingly, outside of the
102 order *Nidovirales*, the only other known RNA virus-encoded 3'-to-5' exoribonucleases are found
103 in the *Arenaviridae* family of viruses. Lassa fever virus nucleoprotein ExoN is not thought to
104 participate in fidelity regulation, but rather it participates in immune evasion by degrading
105 dsRNA and thereby prevents antigen-presenting cell-mediated NK cell activation (18-20).
106 Recently, in the *Alphacoronavirus* transmissible gastroenteritis virus (TGEV), a mutation in the
107 nsp14 ExoN zinc finger was shown to generate lower levels of dsRNA compared to wild-type
108 (WT) TGEV. However, in that study viruses with mutations in ExoN active site motifs were
109 non-viable and therefore, could not be directly tested for effects on innate immunity (21).
110 Here, we demonstrate that viruses lacking ExoN activity were sensitive to the effects of
111 IFN pretreatment. In addition, for viruses lacking ExoN activity, replication was restricted in

112 wild-type bone marrow derived macrophages (B6, BMMs) but restored in interferon alpha/beta
113 receptor deficient (IFNAR-/-) BMMs. Despite an increased sensitivity to the effects of IFN
114 treatment, MHV ExoN mutants failed to induce detectable IFN-β gene expression or RNase L-
115 mediated ribosomal RNA (rRNA) degradation and only a limited decrease in viral RNA
116 accumulation was observed. Finally, ExoN(-) virus replicated in the presence of an IFN-β-
117 mediated antiviral state had both a decreased specific infectivity and decreased relative fitness
118 compared to untreated ExoN(-) virus. Thus, nsp14 ExoN appears to block or correct the
119 restriction of MHV infection by an IFN-mediated mechanism that may involve damaging
120 nascent viral RNA and affecting subsequent infectivity.
121

RESULTS

Viruses lacking ExoN activity are sensitive to the effects of IFN-β. Binding of type I interferon to the IFNAR receptor on the cell surface leads to a Jak/STAT signaling cascade that ultimately results in the up-regulation and expression of hundreds of antiviral ISGs (4). In addition, WT-MHV replication has been shown to be relatively resistant to the effects of IFN (1, 3, 22). To determine whether the ExoN activity of MHV nsp14 was required for resistance to IFN, we pretreated murine delayed brain tumor (DBT) cells with increasing concentrations of mouse IFN-β for 18 h prior to infecting with WT-MHV or ExoN(-) virus at a multiplicity of infection (MOI) of 1 plaque-forming unit (PFU) per cell (Fig. 1A). In response to IFN-β pretreatment, WT-MHV viral titer decreased by approximately 1 $\log_{10}$ as previously reported (1). In contrast, ExoN(-) viral titer demonstrated a dose-dependent decrease and resulted in an approximately 3 $\log_{10}$ decrease in viral titer relative to untreated ExoN(-) viral titers. The ExoN activity of nsp14 is conferred by active site residues present in 3 different motifs within the ExoN domain (23). Therefore, to determine whether the observed sensitivity to IFN-β pretreatment for ExoN(-) virus in Fig. 1A was due specifically to the absence of ExoN activity in nsp14, we engineered and recovered a virus encoding only an aspartic acid to alanine substitution in Motif III [ExoN3(-)]. Previously, we have demonstrated that viruses lacking ExoN activity have decreased replication fidelity and are sensitive to the RNA mutagen 5-fluorouracil (5-FU) (16). Hence, 5-FU sensitivity is an *in vitro* indicator of ExoN activity. Therefore, first, we tested whether ExoN3(-) and ExoN(-) demonstrated similar sensitivity to 5-FU to ensure that the ExoN activity of ExoN3(-) virus had been ablated. Similar to ExoN(-), ExoN3(-) viral replication in cells treated with increasing concentrations of 5-FU demonstrated a dose-dependent decrease in viral titer relative to vehicle treated cells (Fig. 1B). Further, ExoN(-)

and ExoN3(-) displayed similar sensitivities to pre-treatment with 100 or 500 U/mL IFN-β following infection at an MOI of 1 PFU/cell (Fig. 1C). Thus, these data suggest nsp14 ExoN activity is required for resistance to the effects of IFN-β pretreatment and subsequent up-regulation and expression of ISGs.

Increased replication capacity does not confer resistance to the effects of IFN-β pretreatment for viruses lacking ExoN activity. ExoN(-) virus demonstrates an approximately 2 h delay in exponential replication and a 1 $\log_{10}$ decrease in peak titer relative to WT-MHV (15). Therefore, we tested whether the IFN sensitivity phenotype observed for ExoN(-) and ExoN3(-) viruses is due to the decreased replication capacity of these viruses. To do so, we utilized an ExoN(-) virus developed by our lab that has been blindly passaged in DBT cells for 250 passages [ExoN(-) P250] (24). The replication capacity of the resulting ExoN(-) P250 virus exceeds that of WT-MHV (Fig. 2A). However, despite increased replication capacity, ExoN(-) P250 demonstrated similar sensitivity to IFN-β pretreatment as ExoN(-) virus (Fig. 2A and B). Hence, the IFN-β sensitivity phenotype of viruses lacking ExoN activity is not dependent on viral replication capacity but instead, is directly associated with a specific function of nsp14 ExoN that is required for efficient replication in the presence of an IFN-β-mediated antiviral state.

Nsp14 ExoN activity is required for replication in wild-type B6 BMMs. We next wanted to test whether ExoN activity was required for IFN resistance in primary innate immune cells, such as BMMs. Replication of WT-MHV in primary BMMs is well described, and data suggest that wild-type B6 BMMs (B6) express many PRRs and ISGs at a higher basal level than many mouse

cell lines (3, 25, 26). In contrast, BMMs lacking the IFNAR receptor (IFNAR-/-) have lower basal and expressed levels of ISGs; thus, making B6 and IFNAR-/- BMMs excellent cell types for interrogating the role of ExoN activity on viral replication and antagonism of the innate immune response (25). BMMs from B6 or IFNAR-/- mice were generated and infected with WT-MHV or ExoN(-) virus at an MOI of 1 PFU/cell. Samples were harvested at the indicated time points, and viral titers were determined by plaque assay (Fig. 3A). WT-MHV replication increased gradually in both B6 and IFNAR-/- BMMs at each time-point post-infection. In contrast, ExoN(-) virus replication in B6 BMMs was only detectable at 6 and 9 h post-infection. However, when IFNAR-/- BMMs were infected with ExoN(-) virus, viral titers were partially restored and increased at each time point post-infection. To further test the replication of viruses lacking ExoN activity and the effect of an increased replication capacity in BMMs, B6 and IFNAR-/- BMMs were infected with WT-MHV or ExoN(-) P250 viruses at an MOI of 1 PFU/cell. Similar to Fig. 3A, WT-MHV viral titers steadily increased in B6 and IFNAR-/- BMMs at each time-point post-infection (Fig. 3B). However, similar to ExoN(-) virus, ExoN(-) P250 virus replication in B6 BMMs was restricted and not detected beyond 9 h post-infection. In addition, ExoN(-) P250 virus replication in IFNAR-/- BMMs was restored to similar levels as WT-MHV. These data show that ExoN activity is required for replication in B6 BMMs. Further, they suggest that restriction of ExoN(-) or ExoN(-) P250 is mediated by a gene or genes down-stream of IFNAR.

Loss of ExoN activity does not result in the induction of IFN and replication is not rescued by RNase L/PKR deficiency. Upon detection of a pathogen-associated molecular pattern (PAMP) by innate sensors, signaling pathways lead to transcription factor activation and nuclear

translocation resulting in expression of IFN-β mRNA (4). WT-MHV is well known to prevent or delay the induction of IFN expression (3, 22). However, ExoN activity may help prevent the detection of a PAMP, namely dsRNA, which has been shown to be increased in an nsp15 EndoU mutant (12). Therefore, to determine whether the loss of ExoN activity resulted in the generation and subsequent detection of a PAMP, we determined the level of IFN-β gene expression in DBT cells infected with mock, WT-MHV, ExoN(-), or ExoN(-) P250 virus at an MOI of 0.1 PFU/ cell (Fig. 4A). In addition, we infected DBT cells with Sendai virus (SenV), a positive control and a potent inducer of IFN, at an MOI of 200 HA units/ml. SenV infection resulted in IFN expression by 3 h post-infection and peaked between 9 and 12 h post-infection prior to returning nearly to mock infected levels by 24 h post-infection, demonstrating that DBT cells are capable of expressing IFN-β. In contrast, no CoV infection, regardless of whether intact ExoN activity was present, resulted in IFN-β gene expression over mock-infected cells with the exception of WT-MHV at 3 h post-infection. Further, upon detection of dsRNA by OAS and subsequent activation of RNase L, viral and cellular RNAs are degraded as an antiviral mechanism (4). To determine whether infection with ExoN(-) virus activates RNase L, DBT cells were pretreated with 0 or 50 U/ml mouse IFN-β and infected with WT-MHV or ExoN(-) virus at an MOI of 1 PFU/cell or transfected with 25μg/ml poly I:C, a dsRNA surrogate. At the indicated times post-infection, cell lysates were harvested, total RNA extracted, and the integrity of cellular rRNA determined using a bioanalyzer (Fig. 4B). Transfection of DBT cells with poly I:C resulted in rRNA degradation, whereas, infection of DBT cells with WT-MHV or ExoN(-) virus did not result in rRNA degradation under any tested conditions. Lastly, when B6 or RNase L -/- / PKR -/- BMMs (RL -/- / PKR -/-) were infected with ExoN(-) virus, replication was restricted (Fig. 4C). In contrast to infection of B6 BMMs, ExoN(-) viral titer from RL -/- / PKR -/- BMMs was detectable at 12 and

24 h post-infection. However, viral yield was minimal. These data suggest that loss of nsp14 ExoN activity does not lead to the transcriptional activation of IFN-β or a notable dsRNA sensor such as OAS/RNase L during infection of DBT cells. In addition, BMMs deficient in the antiviral effectors RNase L and PKR were not sufficient to restore ExoN(-) viral replication.

IFN treatment does not substantially alter ExoN(-) viral RNA accumulation or particle release. Since ExoN activity is required for resistance to IFN but had no effect on IFN induction, we sought to discern the stage of viral replication that was restricted by IFN-β treatment. To determine the effect of IFN-β pretreatment on viral RNA accumulation, DBT cells were pretreated with 0 or 100 U/ml mouse IFN-β for 18 h and subsequently infected with WT-MHV or ExoN(-) virus at an MOI of 1 PFU/cell. At the indicated times post-infection, the number of genomic RNA copies present were determined by qRT-PCR. IFN-β pretreatment had minimal effect on the accumulation of WT-MHV genomic RNA (Fig. 5A). Whereas ExoN(-) genomic RNA accumulation is delayed relative to WT-MHV (15), pretreatment with IFN-β did not substantially decrease ExoN(-) genomic RNA levels (Fig. 5A). In addition, we determined the effects of IFN-β pretreatment on the levels of subgenomic viral RNA. For both WT-MHV and ExoN(-) viruses, IFN-β pretreatment did not substantially reduce subgenomic RNA levels at any time-point (Fig. 5B). These data indicate that IFN pretreatment did not result in the gross degradation or inhibition of ExoN(-) or ExoN(-) P250 viral RNA accumulation. While slight reductions in viral RNA could explain a small portion of the IFN phenotype, these data suggest that decreased replication or transcription is not the primary driver of ExoN(-) IFN sensitivity.

Since pretreatment of DBT cells with IFN-β does not grossly alter ExoN(-) viral RNA accumulation but does reduce ExoN(-) viral titers, we sought to determine whether IFN

pretreatment prior to infection resulted in a measurable difference in the number of viral particles released from WT-MHV or ExoN(-) infected cells. DBT cells were pretreated with 0 or 100 U/ml mouse IFN-β for 18 h and subsequently infected with WT-MHV or ExoN(-) virus at an MOI of 1 PFU/cell. At 12 h post-infection, cell culture supernatants were harvested and an aliquot of two equal volumes were removed. From the first volume of each sample, RNA was extracted and used to perform one-step qRT-PCR to determine the number of genome RNAs present, and hence, the number of genome RNA containing particles present in the given volume of supernatant (Fig. 5C). The second volume was saved for a plaque assay as described below. Pretreatment of cells with IFN-β resulted in approximately a 1 $\log_{10}$ decrease in the number of supernatant viral particles for both WT-MHV and ExoN(-) viruses compared to the number of supernatant viral particles from untreated cells, demonstrating that IFN pretreatment affects the release of WT-MHV and ExoN(-) virus particles equally (Fig. 5D). Thus, these data suggest that IFN pretreatment does not restrict the primary replication of viruses lacking ExoN activity, but rather, renders them potentially inadequate for subsequent infection.

ExoN(-) virus progeny generated in the presence of an IFN induced-antiviral state have decreased specific infectivity and fitness upon subsequent infection. While many ISGs antagonize viral replication, some could alter the infectivity of progeny particles (27, 28). To test whether IFN pretreatment affected the infectivity of ExoN(-) viral particles, the remaining cell culture supernatant volume described above was used to perform a plaque assay to determine the number of PFUs present (data not shown). Using the number of particles determined in Fig. 5C and the number of PFUs present in an equivalent volume; we calculated the specific infectivity, or particle-to-PFU ratio, of each virus generated under each condition (Fig. 6A). Regardless of

IFN-β pretreatment during the initial infection, the specific infectivity of WT-MHV was approximately 10 particles per 1 PFU upon subsequent infection. Infection of untreated DBT cells with ExoN(-) virus resulted in a similar particle to PFU ratio as WT-MHV during subsequent infection. In contrast, when DBT cells were pretreated with IFN-β prior to initial infection with ExoN(-) virus, the resulting specific infectivity of ExoN(-) virus was 100 particles per 1 PFU, a significant decrease in specific infectivity. Therefore, ExoN(-) virus generated in the presence of an IFN-β-mediated antiviral state requires 10-fold more genome RNA containing particles to generate 1 PFU than WT-MHV generated in cells pretreated with or without IFN or ExoN(-) virus generated in untreated cells. These data suggest that the IFN-mediated restriction of ExoN(-) virus in DBT cells occurs at the level of subsequent infection by reducing particle infectivity.

Next, we tested whether the effects of IFN on ExoN(-) viruses were intrinsic to the viruses produced. To do so, we performed a co-infection assay, which utilized WT-MHV and ExoN(-) viruses harboring 10 silent mutations in the nsp2-coding region (WT silent and ExoN(-) silent, respectively) along with WT-MHV and ExoN(-) viruses. The genome RNAs of the silent viruses are recognized exclusively by a separate probe than the one used to detect the "WT" nsp2 probe-binding region of WT-MHV or ExoN(-) viruses (24). Thus, allowing WT silent and ExoN(-) silent to act as internal controls for a co-infection assay under identical conditions. DBT cells were pretreated with 0 or 100 U/ml mouse IFN-β for 18 h and subsequently infected with WT-MHV or ExoN(-) virus at an MOI of 1 PFU/cell. At 12 h post-infection, total cell culture supernatants were collected. The number of viral particles present in a representative aliquot was determined from purified virion genome RNA by one-step qRT-PCR. In addition, we determined the number of genome RNA containing particles in an equivalent volume of WT silent or ExoN(-

283) silent viral p1 stock tubes. Using the calculated number of genome RNA-containing viral
284 particles, we added an equal number of WT-MHV viral particles generated in the absence of IFN
285 pretreatment to WT silent viral particles and an equal number of WT-MHV viral particles
286 generated in the presence of IFN pretreatment to WT silent viral particles. This same set-up was
287 repeated for ExoN(-) viral particles generated in the presence or absence of IFN pretreatment
288 with ExoN(-) silent viral particles. Finally, each combination was used to infect a fresh
289 monolayer of untreated DBT cells. At 24 h post-co-infection, total cell culture supernatants were
290 collected and virion genome RNA was extracted to determine the number of supernatant viral
291 particles present from each combination of input viruses by one-step qRT-PCR and is reported as
292 the change in fitness relative to the respective silent virus standard (Fig. 6B). WT-MHV particles
293 generated in the presence of IFN pretreatment generated a similar number of viral particles over
294 the course of co-infection as WT-MHV generated in the absence of IFN pretreatment relative to
295 their respective silent standards. However, the number of viral particles present from ExoN(-)
296 virus generated in the presence of IFN pretreatment during the course of co-infection decreased
297 by approximately 1.5 $\log_{10}$ in comparison with ExoN(-) viral particles generated in the absence
298 of IFN pretreatment relative to their respective silent standards. These data indicate that a loss in
299 nsp14 ExoN activity sensitizes viruses to IFN pretreatment and reduces the infectivity and fitness
300 of progeny during subsequent rounds of infection in the absence of an antiviral state.
301
302 **DISCUSSION**
303 CoVs encode multiple IFN antagonists that prevent the induction of or mediate resistance to the
304 innate immune response; thus, allowing efficient viral replication early during infection (3).
305 Moreover, an insufficient innate immune response has been proposed to be a major contributor

306 to SARS-CoV pathogenesis (29). In this study, we sought to determine the contributions of
307 nsp14 ExoN activity in the induction of and resistance to the innate immune response. We
308 demonstrate that ExoN(-) virus is sensitive to pretreatment with IFN-β. Because ExoN3(-) and
309 ExoN(-) P250 viruses were also sensitive to the effects of IFN, we conclude that IFN sensitivity
310 is specifically due to loss of ExoN activity.
311 Because the ExoN activity of the Lassa fever virus nucleoprotein degrades dsRNA
312 intermediates (18, 19), we hypothesized that CoV nsp14 ExoN could function in a similar
313 manner. If nsp14 ExoN is degrading viral dsRNA, ExoN inactivation should increase
314 intracellular dsRNA accumulation, resulting in a concomitant increase in IFN-β expression or
315 activation of RNase L during infection. We neither observed IFN-β up-regulation nor RNase L
316 activation over the course of ExoN(-) virus infection (Fig. 4A and B), and rRNA was intact at all
317 time-points tested (Fig. 4B). Therefore, at least two possible explanations exist: 1.) ExoN does
318 not function to degrade dsRNA or 2.) ExoN does degrade dsRNA, but the detection of this
319 PAMP is unchanged during ExoN(-) virus infection due to sufficient antagonism by other CoV
320 proteins. Basal OAS expression levels correlate with RNase L activation (30). Thus, we
321 pretreated DBTs with IFN-β to up-regulate OAS and RNase L expression. However, rRNA
322 degradation was only observed in cells transfected with poly I:C (Fig. 4B). Further, nsp15
323 EndoU and NS2 phosphodiesterase activities were intact during all of our experiments. Thus, it
324 is possible that in the absence of nsp14 ExoN activity, other CoV innate antagonists were
325 sufficient to prevent innate detection by the cell or prevent the induction of a detectable signal in
326 the experiments we performed. However, one would expect the endonucleolytic products of
327 nsp15 to be smaller dsRNAs that could still activate RIG-I or MDA5, similar to RNase L
328 products, unless another RNA degradation mechanism were in place (4, 31). In addition, despite

329 an intact NS2 phosphodiesterase, nsp15 mutants still activate RNase L-mediated rRNA
330 degradation (12). Lastly, when RNaseL -/- / PKR -/- BMMs were infected with ExoN(-) virus,
331 viral replication was not rescued, suggesting that RNase L and PKR are not required for ExoN(-)
332 virus restriction (Fig. 4C). Moreover, these data suggest dsRNA is not detected and the antiviral
333 effectors RNaseL and PKR are not activated during ExoN(-) virus infection.
334 During our study, Becares et al. reported that a TGEV nsp14 zinc-finger mutant
335 modulated the innate immune response of swine testis cells by reducing the levels of dsRNA and
336 induction of IFN (21). Unlike TGEV, *Betacoronaviruses* such as SARS-CoV and MHV, do not
337 induce IFN expression in most cell types (1-3) (Fig.4A). Interestingly, TGEV ExoN active site
338 mutants were non-viable; although, this is not the first report of non-viable ExoN active site
339 residue mutants in *Alphacoronaviruses* (21). In the initial report of CoV nsp14 ExoN activity,
340 human CoV 229E ExoN active site mutants were also non-viable, suggesting a common essential
341 function for nsp14 ExoN in *Alphacoronavirus* replication and/or innate antagonism (13).
342 Altogether, the possibility of a common innate immune antagonism function for nsp14 across
343 *Alpha*- and *Beta*-CoVs is apparent but clearly differing requirements exist that may be dependent
344 on the CoV genus and cell types used.
345 Our results clearly demonstrate that viruses lacking ExoN activity are sensitive to IFN-β
346 pretreatment in a dose-dependent manner (Fig. 1A,C and Fig. 2). Further, replication of viruses
347 lacking ExoN activity was dependent on the capacity of BMMs to express genes downstream of
348 IFNAR signaling (Fig. 3). This is due to the fact that B6 and IFNAR-/- cells have different levels
349 of basal ISG expression and thus, two very different intracellular environments for viral
350 replication to occur (3, 25, 26). In IFNAR-/- BMMs, ExoN(-) and ExoN(-) P250 virus replication
351 capacity was restored to levels approaching or exceeding WT-MHV levels (Fig. 3). Further, our

specific infectivity (Fig. 6A) and co-infection (Fig. 6B) data show that ExoN(-) virus generated in the presence of an antiviral state is less viable upon subsequent infection. Altogether, our results suggest that an ISG or ISGs is (are) acting on ExoN(-) virus, specifically resulting in progeny that are less viable upon subsequent infection. Thus, it will be interesting to determine the specific ISG or ISGs responsible for mediating the observed restriction. In addition, it will be important to determine whether a greater proportion of the incoming ExoN(-) viral particles are strictly non-viable or whether cells are now sensing the progeny ExoN(-) viruses and inhibiting replication. Due to the pleiotropic nature of IFN-β, more than one mechanism may be acting. To date, the majority of our understanding of nsp14 ExoN activity is in the context of proofreading during CoV replication (13, 15, 16, 32). CoVs lacking ExoN activity demonstrate an increase in mutation frequency relative to WT (15, 16). Thus, it is possible that ExoN(-) virus replication in IFN pretreated cells results in further alteration of ExoN(-) virus mutation frequency. Certainly, an increase or decrease in mutation frequency could impair viral replication during a subsequent infection. In addition, an ISG may act to hypermutate the large CoV genome in the absence of ExoN activity, rendering viral progeny less viable. ISGs that increase viral mutation frequency have been described such as adenosine deaminase acting on RNA 1 (ADAR1) and apolipoprotein B mRNA editing enzyme, catalytic polypeptide-like 3G (APOBEC3G) (27, 28). Further, another ISG, SAMHD1, may inhibit HIV replication by limiting nucleotide pools, a known contributor to increased viral mutation frequency (33-35). Moreover, other possible mechanisms outside of altered mutation frequency exist. For instance, in the absence of ExoN activity, terminal RNA modifications, recombination, and/or replicase protein interactions mediated by nsp14 ExoN may be disrupted to a greater extent in the presence of an IFN-β-mediated antiviral state.

375 Since CoVs encode the largest genome known for RNA viruses, they have the luxury of
376 encoding multiple IFN antagonists that limit the capacity of a cell to detect and respond to
377 infection. Collectively, our data suggest that MHV nsp14 ExoN activity is a contributor to CoV
378 innate immune antagonism. We clearly demonstrate that viruses lacking ExoN activity are
379 sensitive to the effects of an IFN-β-mediated antiviral state. Further, our data reveal a critical role
380 for nsp14 ExoN activity in CoV replication and provide additional rationale for targeting nsp14
381 ExoN activity as a means of viral attenuation. Our future studies will probe the specific
382 mechanism of restriction for viruses lacking ExoN activity and assess how the requirement of
383 ExoN activity for resistance to innate immunity can be utilized for treatment during human
384 coronavirus infections.
385
386 **MATERIALS AND METHODS**
387 **Cell culture.** Murine delayed brain tumor (DBT) cells (36) and baby hamster kidney 21 cells
388 expressing the MHV receptor (BHK-R) (37) were maintained at 37°C in Dulbecco's modified
389 Eagle medium (DMEM; Gibco) supplemented with 10% fetal bovine serum (FBS; Invitrogen),
390 100 U/ml penicillin and streptomycin (Gibco), and 0.25 μg/ml amphotericin B (Corning). BHK-
391 R cells were further supplemented with 0.8 mg/ml of G418 (Mediatech).
392
393 **Cloning, recovery, and verification of mutant viruses.** Recombinant MHV strain A59
394 (GenBank accession number AY910861) has been previously described (37). ExoN(-) (nsp14
395 D89A and E91A) has been previously described (15). To generate ExoN(-) P250 virus, sub-
396 confluent monolayers of DBT cells in 25cm^2 flasks were infected using the ExoN(-) parental
397 stock and blindly passaged for a total of 250 passages (24). For ExoN3(-) virus (nsp14 D272A),

site-directed mutagenesis was used to engineer point mutations in the MHV genome cDNA F fragment plasmid using the MHV infectious clone reverse genetics system (37). ExoN3(-) mutant virus was recovered using BHK-R cells following electroporation of *in vitro*-transcribed genomic RNA. Recovered ExoN3(-) virus was sequenced (GenHunter Corporation, Nashville, TN) to verify the engineered mutations were present and to ensure that no additional mutations were introduced.

Interferon-β sensitivity assays. Sub-confluent DBT cells were treated for 18 h with the indicated concentrations of mouse IFN-β (PBL Assay Science) prior to infection with virus at a multiplicity of infection (MOI) of 1 plaque-forming unit (PFU) per cell at 37°C for 45 min. After incubation, inocula were removed, cells were washed with PBS, and fresh medium was added. Cell culture supernatants were collected at 12 h post-infection, and viral titers were determined by plaque assay (15).

5-FU sensitivity assays. Sub-confluent DBT cells were treated with DMEM supplemented to contain the indicated concentrations of 5-fluorouracil [(5-FU), Sigma] or DMSO alone at 37°C for 30 min. After incubation, drug was removed and cells were infected with virus at an MOI of 1 PFU/cell at 37°C for 1 h. Inocula were removed, and cells were incubated in medium containing 5-FU or DMSO. Cell culture supernatants were collected at 12 h post-infection, and viral titers were determined by plaque assay.

Virus replication kinetics. Bone-marrow derived macrophages (BMMs) were generated from the hind limbs of WT, IFNAR-/-, or RNaseL-/-/PKR-/- C57/B6 mice as previously described

(11). BMMs were infected with virus at an MOI of 1 PFU/cell at 37°C for 1 h. After incubation, inocula were removed, cells were washed with 3 times with PBS, and fresh medium was added. At the indicated times post-infection, cell culture supernatant aliquots were collected and viral titers determined by plaque assay.

Interferon-β induction assays. Sub-confluent DBT cells were infected with mock, WT, ExoN(-), or ExoN(-) P250 virus at an MOI of 0.1 PFU/cell or with Sendai virus (SenV) at an MOI of 200 HA (hemagglutination units)/ml at 37°C for 45 min. Inocula were removed, cells were washed with PBS, and fresh medium was added. At the indicated times post-infection, cell culture supernatants were removed and cell lysates were harvested by adding 1ml TRIzol reagent. Total RNA present in the lysates was purified using the phenol/chloroform method. cDNA was generated by reverse transcriptase-polymerase chain reaction (RT-PCR) using 1µg of total RNA as previously described (16). Mouse IFN-β expression levels were determined relative to GAPDH by qPCR using the Applied Biosciences 7500 Real-Time PCR System with Power SYBR Green PCR Master Mix and IFN-β primers: FWD: 5'-TCCGCCCTGTAGGTGAGGTTGAT-3' and REV: 5'-GTTCCTGCTGTGCTTCTCCACCA-3' and GAPDH primers previously reported (16).

Determination of rRNA integrity. Sub-confluent monolayers of DBT cells were treated with 0 or 50 U/ml mouse IFN-β for 18 h prior to being infected with virus at an MOI of 1 PFU/cell at 37°C for 45 min. After incubation, inocula were removed, cells were washed with PBS, and fresh medium was added. At the indicated times post-infection, cell culture supernatants were removed and total RNA was harvested by adding 1ml TRIzol reagent. For a positive control,

444 cells were transfected with 25ug/ml polyI:C (Sigma) using Lipofectamine 2000 (Thermo Fisher
445 Scientific). Total RNA from all samples was purified using the Purelink RNA Mini Purification
446 System (Life Technologies) by following the manufacturers instructions. Upon purification, total
447 RNA was analyzed on an Agilent Bioanalyzer by the Vanderbilt VANTAGE core facility and
448 the rRNA integrity reported.
449
450 **Quantification of viral genomic RNA by qRT-PCR.** The quantification of viral genomic RNA
451 has been previously described (14). Briefly, an RNA standard was prepared using the MHV A
452 fragment (37) and a standard curve was generated using 10-fold dilutions from 10^3 to 10^8 copies.
453 A 5' 6-carboxyfluorescein (FAM)-labeled probe (5'-TTCTGACAACGGCTACACCCAACG-3'
454 [Biosearch Technologies]) was used with forward (5'-AGAAGGTTACTGGCAACTG-3') and
455 reverse (5'-TGTCCACGGCTAAATCAAAC-3') nsp2 specific primers. The final volume for
456 each reaction was 20 µl with 150 nM probe, 900 nM each primer, 2 µl sample RNA, and 10 µl
457 2X ToughMix, one-step, low ROX enzyme mix (Quantas) per reaction. Samples were quantified
458 using an Applied Biosciences 7500 Real-Time PCR System with the conditions 55°C for 10 min,
459 95°C for 5 min, 95°C for 30 s, and 60°C for 1 min, with the last two steps repeated 40 times. The
460 standard curve was plotted using GraphPad Prism 6 software, and genomes/µl were calculated.
461
462 **Quantification of subgenomic RNA by qPCR.** Sub-confluent DBT cells were treated with 0 or
463 100 U/mL mouse IFN-β for 18 h prior to being infected with virus at an MOI of 1 PFU/cell at
464 37°C for 45 min. After incubation, inocula were removed, cells were washed with PBS, and
465 fresh medium was added. At the indicated times post-infection, cell culture supernatants were
466 removed and total RNA was harvested by adding 1ml TRIzol reagent. Total RNA was extracted

using the Purelink RNA mini purification system by following the manufacturers instructions. cDNA was generated by RT-PCR using 1ug of total RNA as previously described (16). Primers used to detect subgenomic nucleocapsid and GAPDH gene expression have been reported (16, 38). Subgenomic (N) expression levels relative to GAPDH were determined using the Applied Biosciences 7500 Real-Time PCR System with Power SYBR Green PCR Master Mix.

Determination of specific infectivity. Sub-confluent monolayers of DBT cells were infected with virus at an MOI of 1 PFU/cell at 37°C for 45 min. After incubation, inocula were removed, cells were washed with PBS, and fresh medium was added. At 12 h post-infection, cell culture supernatants were collected, and viral titers were determined by plaque assay. Supernatants also were used for RNA genome isolation by adding 100 µl supernatant to 900 µl TRIzol reagent, chloroform extraction by phase separation, and final purification using the PureLink RNA Mini Purification System. Genome RNA was quantified using one-step qRT-PCR as described above, and the particle to PFU ratio was calculated.

Co-infection assay. Sub-confluent monolayers of DBT cells were treated with 0 or 100 U/ml mouse IFN-β for 18 h prior to being infected with virus at an MOI of 1 PFU/cell at 37°C for 45 min. After incubation, inocula were removed, cells were washed with PBS, and fresh medium was added. At 12 h post-infection, cell culture supernatants were removed and 100 µl of supernatant was added to 900 µl TRIzol reagent. Viral genome RNA was purified and the number of viral genome RNA copies present relative to an RNA standard curve were determined as described above. Based on the number of viral genome RNA copies determined by qRT-PCR, an equal number of virus particles from each virus and each condition were combined with an

equal number of WT silent or ExoN(-) silent virus particles, respectively. WT silent and ExoN(-) silent viruses were engineered to harbor 10 silent mutations in the probe-binding region of nsp2, allowing separate detection from WT-MHV or ExoN(-) virus genomes, respectively, using a separate probe upon co-infection (24). Next, a fresh, sub-confluent monolayer of DBT cells were co-infected with each combination of viruses at 37°C for 45 min. After incubation, inocula were removed, cells were washed with PBS, and fresh medium was added. At 24 h post-infection, cell culture supernatants were removed and 100 µl of supernatant was added to 900 µl TRIzol reagent. Viral genome RNA was purified. The number of viral genome RNA copies of both reference and silent viruses were determined relative to the appropriate standard curve. The number of viral genome RNA copies relative to the number of silent virus genome RNA copies was determined for each virus and condition. Values are reported as the change in fitness relative to the silent virus.

Statistical analysis. Statistical tests were applied as noted in the respective figure legends and were determined using GraphPad Prism 6 software (La Jolla, CA).

ACKNOWLEDGMENTS

We thank members of the Vanderbilt Technologies for Advanced Genomics (VANTAGE) core for rRNA integrity determination services. We thank fellow members of the Denison and Weiss laboratories, specifically Maria Agostini, for helpful discussions. This work was supported by Public Health Service awards T32 HL07751 (J.B.C.) from the National Heart, Lung, and Blood Institute, R01 AI108197 (M.R.D.), and R01 AI104887 (S.R.W.) from the National Institute of Allergy and Infectious Diseases. Additional support was provided by the Elizabeth B. Lamb

513 Center for Pediatric Research.

514

REFFERENCES

1. **Roth-Cross JK**, **Martínez-Sobrido L**, **Scott EP**, **García-Sastre A**, **Weiss SR**. 2007. Inhibition of the alpha/beta interferon response by mouse hepatitis virus at multiple levels. J Virol **81**:7189–7199.
2. **Frieman M**, **Heise M**, **Baric R**. 2008. SARS coronavirus and innate immunity. Virus Res. **133**:101–112.
3. **Rose KM**, **Weiss SR**. 2009. Murine Coronavirus Cell Type Dependent Interaction with the Type I Interferon Response. Viruses **1**:689–712.
4. **Schneider WM**, **Chevillotte MD**, **Rice CM**. 2014. Interferon-stimulated genes: a complex web of host defenses. Annu. Rev. Immunol. **32**:513–545.
5. **Kamitani W**, **Narayanan K**, **Huang C**, **Lokugamage K**, **Ikegami T**, **Ito N**, **Kubo H**, **Makino S**. 2006. Severe acute respiratory syndrome coronavirus nsp1 protein suppresses host gene expression by promoting host mRNA degradation. Proc. Natl. Acad. Sci. U.S.A. **103**:12885–12890.
6. **Zhang R**, **Li Y**, **Cowley TJ**, **Steinbrenner AD**, **Phillips JM**, **Yount BL**, **Baric RS**, **Weiss SR**. 2015. The nsp1, nsp13, and M proteins contribute to the hepatotropism of murine coronavirus JHM.WU. J. Virol. **89**:3598–3609.
7. **Devaraj SG**, **Wang N**, **Chen Z**, **Chen Z**, **Tseng M**, **Barretto N**, **Lin R**, **Peters CJ**, **Tseng C-TK**, **Baker SC**, **Li K**. 2007. Regulation of IRF-3-dependent innate immunity by the papain-like protease domain of the severe acute respiratory syndrome coronavirus. J. Biol. Chem. **282**:32208–32221.
8. **Barretto N**, **Jukneliene D**, **Ratia K**, **Chen Z**, **Mesecar AD**, **Baker SC**. 2005. The papain-like protease of severe acute respiratory syndrome coronavirus has deubiquitinating activity. J. Virol. **79**:15189–15198.
9. **Chen Y**, **Cai H**, **Pan J**, **Xiang N**, **Tien P**, **Ahola T**, **Guo D**. 2009. Functional screen reveals SARS coronavirus nonstructural protein nsp14 as a novel cap N7 methyltransferase. Proc Natl Acad Sci USA **106**:3484–3489.
10. **Decroly E**, **Imbert I**, **Coutard B**, **Bouvet M**, **Selisko B**, **Alvarez K**, **Gorbalenya AE**, **Snijder EJ**, **Canard B**. 2008. Coronavirus nonstructural protein 16 is a cap-0 binding enzyme possessing (nucleoside-2'O)-methyltransferase activity. J. Virol. **82**:8071–8084.
11. **Zhao L**, **Jha BK**, **Wu A**, **Elliott R**, **Ziebuhr J**, **Gorbalenya AE**, **Silverman RH**, **Weiss SR**. 2012. Antagonism of the interferon-induced OAS-RNase L pathway by murine coronavirus ns2 protein is required for virus replication and liver pathology. Cell Host Microbe **11**:607–616.
12. **Kindler E**, **Gil-Cruz C**, **Spanier J**, **Li Y**, **Wilhelm J**, **Rabouw HH**, **Züst R**, **Hwang M**, **V'kovski P**, **Stalder H**, **Marti S**, **Habjan M**, **Cervantes-Barragan L**, **Elliot R**, **Karl N**, **Gaughan C**, **van Kuppeveld FJM**, **Silverman RH**, **Keller M**, **Ludewig B**, **Bergmann CC**, **Ziebuhr J**, **Weiss SR**, **Kalinke U**, **Thiel V**. 2017. Early endonuclease-mediated evasion of RNA sensing ensures efficient coronavirus replication. PLoS Pathog. **13**:e1006195.
13. **Minskaia E**, **Hertzig T**, **Gorbalenya AE**, **Campanacci V**, **Cambillau C**, **Canard B**, **Ziebuhr J**. 2006. Discovery of an RNA virus 3"->5" exoribonuclease that is critically involved in coronavirus RNA synthesis. Proc Natl Acad Sci USA **103**:5108–5113.
14. **Case JB**, **Ashbrook AW**, **Dermody TS**, **Denison MR**. 2016. Mutagenesis of S-Adenosyl-l-Methionine-Binding Residues in Coronavirus nsp14 N7-Methyltransferase

Demonstrates Differing Requirements for Genome Translation and Resistance to Innate Immunity. J. Virol. **90**:7248–7256.

15. **Eckerle LD**, **Lu X**, **Sperry SM**, **Choi L**, **Denison MR**. 2007. High fidelity of murine hepatitis virus replication is decreased in nsp14 exoribonuclease mutants. J Virol **81**:12135–12144.
16. **Smith EC**, **Blanc H**, **Vignuzzi M**, **Denison MR**. 2013. Coronaviruses lacking exoribonuclease activity are susceptible to lethal mutagenesis: evidence for proofreading and potential therapeutics. PLoS Pathog **9**:e1003565.
17. **Graham RL**, **Becker MM**, **Eckerle LD**, **Bolles M**, **Denison MR**, **Baric RS**. 2012. A live, impaired-fidelity coronavirus vaccine protects in an aged, immunocompromised mouse model of lethal disease. Nat Med **18**:1820–1826.
18. **Qi X**, **Lan S**, **Wang W**, **Schelde LM**, **Dong H**, **Wallat GD**, **Ly H**, **Liang Y**, **Dong C**. 2010. Cap binding and immune evasion revealed by Lassa nucleoprotein structure. Nature **468**:779–783.
19. **Hastie KM**, **Kimberlin CR**, **Zandonatti MA**, **MacRae IJ**, **Saphire EO**. 2011. Structure of the Lassa virus nucleoprotein reveals a dsRNA-specific 3“ to 5” exonuclease activity essential for immune suppression. PNAS **108**:2396–2401.
20. **Russier M**, **Reynard S**, **Carnec X**, **Baize S**. 2014. The exonuclease domain of Lassa virus nucleoprotein is involved in antigen-presenting-cell-mediated NK cell responses. J. Virol. **88**:13811–13820.
21. **Becares M**, **Pascual-Iglesias A**, **Nogales A**, **Sola I**, **Enjuanes L**, **Zuñiga S**. 2016. Mutagenesis of Coronavirus nsp14 Reveals Its Potential Role in Modulation of the Innate Immune Response. J. Virol. **90**:5399–5414.
22. **Rose KM**, **Elliott R**, **Martínez-Sobrido L**, **García-Sastre A**, **Weiss SR**. 2010. Murine coronavirus delays expression of a subset of interferon-stimulated genes. J Virol **84**:5656–5669.
23. **Ma Y**, **Wu L**, **Shaw N**, **Gao Y**, **Wang J**, **Sun Y**, **Lou Z**, **Yan L**, **Zhang R**, **Rao Z**. 2015. Structural basis and functional analysis of the SARS coronavirus nsp14-nsp10 complex. PNAS **112**:9436–9441.
24. **Graepel K**, **Lu X**, **Case JB**, **Sexton NR**, **Smith EC**, **Denison MR**. 2017. Proofreading-deficient coronaviruses adapt over long-term passage for increased fidelity and fitness without reversion of exoribonuclease-inactivating mutations. bioRxiv.
25. **Zhao L**, **Rose KM**, **Elliott R**, **Van Rooijen N**, **Weiss SR**. 2011. Cell-type-specific type I interferon antagonism influences organ tropism of murine coronavirus. J. Virol. **85**:10058–10068.
26. **Zhao L**, **Birdwell LD**, **Wu A**, **Elliott R**, **Rose KM**, **Phillips JM**, **Li Y**, **Grinspan J**, **Silverman RH**, **Weiss SR**. 2013. Cell-type-specific activation of the oligoadenylate synthetase-RNase L pathway by a murine coronavirus. J. Virol. **87**:8408–8418.
27. **Tomaselli S**, **Galeano F**, **Locatelli F**, **Gallo A**. 2015. ADARs and the Balance Game between Virus Infection and Innate Immune Cell Response. Curr Issues Mol Biol **17**:37–51.
28. **Neil S**, **Bieniasz P**. 2009. Human immunodeficiency virus, restriction factors, and interferon. J. Interferon Cytokine Res. **29**:569–580.
29. **Gu J**, **Korteweg C**. 2007. Pathology and pathogenesis of severe acute respiratory syndrome. Am. J. Pathol. **170**:1136–1147.
30. **Birdwell LD**, **Zalinger ZB**, **Li Y**, **Wright PW**, **Elliott R**, **Rose KM**, **Silverman RH**,

Weiss SR. 2016. Activation of RNase L by Murine Coronavirus in Myeloid Cells Is Dependent on Basal Oas Gene Expression and Independent of Virus-Induced Interferon. J. Virol. **90**:3160–3172.

31. **Malathi K**, **Dong B**, **Gale M**, **Silverman RH**. 2007. Small self-RNA generated by RNase L amplifies antiviral innate immunity. Nature **448**:816–819.
32. **Bouvet M**, **Imbert I**, **Subissi L**, **Gluais L**, **Canard B**, **Decroly E**. 2012. RNA 3'-end mismatch excision by the severe acute respiratory syndrome coronavirus nonstructural protein nsp10/nsp14 exoribonuclease complex. Proc. Natl. Acad. Sci. U.S.A. **109**:9372–9377.
33. **Lahouassa H**, **Daddacha W**, **Hofmann H**, **Ayinde D**, **Logue EC**, **Dragin L**, **Bloch N**, **Maudet C**, **Bertrand M**, **Gramberg T**, **Pancino G**, **Priet S**, **Canard B**, **Laguette N**, **Benkirane M**, **Transy C**, **Landau NR**, **Kim B**, **Margottin-Goguet F**. 2012. SAMHD1 restricts the replication of human immunodeficiency virus type 1 by depleting the intracellular pool of deoxynucleoside triphosphates. Nat. Immunol. **13**:223–228.
34. **Hrecka K**, **Hao C**, **Gierszewska M**, **Swanson SK**, **Kesik-Brodacka M**, **Srivastava S**, **Florens L**, **Washburn MP**, **Skowronski J**. 2011. Vpx relieves inhibition of HIV-1 infection of macrophages mediated by the SAMHD1 protein. Nature **474**:658–661.
35. **Sanjuán R**, **Domingo-Calap P**. 2016. Mechanisms of viral mutation. Cell. Mol. Life Sci. **73**:4433–4448.
36. **Chen W**, **Baric RS**. 1996. Molecular anatomy of mouse hepatitis virus persistence: coevolution of increased host cell resistance and virus virulence. J. Virol. **70**:3947–3960.
37. **Yount B**, **Denison MR**, **Weiss SR**, **Baric RS**. 2002. Systematic Assembly of a Full-Length Infectious cDNA of Mouse Hepatitis Virus Strain A59. J. Virol. **76**:11065–11078.
38. **Donaldson EF**, **Sims AC**, **Graham RL**, **Denison MR**, **Baric RS**. 2007. Murine hepatitis virus replicase protein nsp10 is a critical regulator of viral RNA synthesis. J. Virol. **81**:6356–6368.

FIGURE LEGENDS

FIG 1. Viruses lacking ExoN activity are sensitive to IFN-β pretreatment. (A) DBT cells were pretreated with the indicated concentrations of mouse IFN-β for 18 h and then infected with WT-MHV or ExoN(-) virus (A) or WT, ExoN(-), or ExoN3(-) virus (C) at an MOI of 1 PFU/cell. At 12 h post-infection, cell culture supernatants were collected and the viral titers present determined by plaque assay. (B) DBT cells were pretreated with the indicated concentrations of 5-FU for 30 min. Following pretreatment, cells were infected with WT, ExoN(-), or ExoN3(-)

646 virus at an MOI of 1 PFU/cell for 45 min., inocula were removed, and fresh medium containing
647 vehicle or the appropriate concentration of 5-FU were added. Cell culture supernatants were
648 harvested 12 h post-infection and viral titers were determined by plaque assay. For each panel,
649 the change in viral titer was calculated by dividing viral titers following the indicated treatment
650 by the untreated controls and error bars indicate SEM (n = 4). Statistical significance compared
651 to WT-MHV is denoted and was determined by Student's *t* –test. *, $P < 0.05$, **$P < 0.01$, *** P
652 < 0.001.
653
654 **FIG 2**. Increased replication capacity does not restore virus resistance to IFN-β. DBT cells were
655 pretreated with the indicated concentrations of mouse IFN-β for 18 h and then infected with WT,
656 ExoN(-), or ExoN(-) P250 virus at an MOI of 1 PFU/cell. At 12 h post-infection, cell culture
657 supernatants were collected and the viral titers present determined by plaque assay. Raw viral
658 titers (A) or the change in viral titers relative to untreated controls (B) are reported. Error bars
659 indicate SEM (n = 4). Statistical significance compared to WT-MHV is denoted and was
660 determined by Student's *t* –test. *, $P < 0.05$, **$P < 0.01$, *** $P < 0.001$.
661
662 **FIG 3**. Replication of viruses lacking ExoN activity is restricted in wild-type B6 BMMs. B6
663 BMMs or IFNAR-/- BMMs were infected with WT-MHV or ExoN(-) virus (A) or WT-MHV or
664 ExoN(-) P250 virus (B) at an MOI of 1 PFU/cell. At the indicated times post-infection, cell
665 culture supernatant aliquots were collected and the viral titers present were determined by plaque
666 assay. For each panel, error bars represent SEM (n = 6 to 7). ND = not detectable.
667
668 **FIG 4**. Loss of ExoN activity does not result in the generation of a detectable PAMP. (A) DBT

669 cells were infected with mock, WT, ExoN(-) or ExoN(-) P250 virus at an MOI of 0.1 PFU/cell or
670 infected with Sendai virus at an MOI of 200 HA units/ml. At the indicated times post-infection,
671 cell culture supernatants were removed, cell lysates were harvested, total RNA was extracted,
672 cDNA was generated, and IFN-β expression relative to GAPDH was determined by qPCR. Error
673 bars indicate SEM (n=4). (B) DBT cells were pretreated for 18 h with 0 or 50U/ml mouse IFN-β
674 and subsequently infected with WT-MHV or ExoN(-) virus or transfected with 25μg/ml poly I:C.
675 At the indicated times post-infection, cell culture supernatants were removed, cell lysates
676 harvested, and total RNA extracted. rRNA integrity was assessed using an Agilent Bioanlyzer.
677 One representative image is shown for each sample from 2 independent experiments. Images
678 spliced for labeling purposes. The averaged RNA integrity values for each condition are
679 reported. (C) B6 BMMs or RL -/- / PKR -/- BMMs were infected with WT-MHV or ExoN(-)
680 virus at an MOI of 1 PFU/cell. At the indicated times post-infection, cell culture supernatant
681 aliquots were collected and the viral titers present were determined by plaque assay. Error bars
682 represent SEM (n = 5). ND = not detectable.
683
684 **FIG 5**. ExoN(-) viral RNA accumulation and particle release is marginally affected by IFN-β
685 pretreatment. DBT cells were pretreated with 0 or 100U/ml mouse IFN-β for 18 h and
686 subsequently infected with WT-MHV or ExoN(-) virus at an MOI of 1 PFU/cell. At the indicated
687 times post-infection, total cell lysates were harvested and RNA was extracted. The viral genomic
688 RNA copies present relative to an RNA standard were determined by one-step qRT-PCR (A) or
689 cDNA was generated and the subgenomic RNA copies relative to GAPDH were determined by
690 qPCR (B). For each panel (A and B), error bars represent SEM (n= 6 to 9). DBT cells were
691 pretreated with 0 or 100U/ml mouse IFN-β for 18 h and subsequently infected with WT-MHV or

692 ExoN(-) virus at an MOI of 1 PFU/cell. At 12 h post-infection, cell culture supernatants were
693 collected. Equivalent volumes of cell culture supernatant for each sample were divided into two
694 samples. For the first cell culture supernatant sample, total RNA was extracted and the number
695 of virion genome RNA copies present (particles) was determined by one-step qRT-PCR (C) or
696 reported as the change in virion genome RNA copies (D). Error bars represent SEM (n = 13 to
697 15). Statistical significance compared to untreated WT-MHV or ExoN(-) infection, respectively,
698 is denoted and was determined by Student's *t* –test. *** $P < 0.001$.
699
700 **FIG 6**. ExoN(-) viruses generated in the presence of an antiviral state have decreased specific
701 infectivity and are less fit relative to untreated. (A) DBT cells were pretreated with 0 or 100U/ml
702 mouse IFN-β for 18 h and subsequently infected with WT-MHV or ExoN(-) virus at an MOI of 1
703 PFU/cell. At 12 h post-infection, cell culture supernatants were collected. Equivalent volumes of
704 cell culture supernatant for each sample were divided into two samples. For the first cell culture
705 supernatant sample, total RNA was extracted and the number of virion genome RNA copies
706 present (particles) was determined by one-step qRT-PCR [Fig. 5C]. For the second cell culture
707 supernatant sample, the viral titer present was determined by plaque assay (PFUs) (data not
708 shown). The particle to PFU ratio for each virus and treatment was calculated by dividing the
709 number of particles by the number of PFUs. Error bars represent SEM (n = 13 to 15). (B) DBT
710 cells were pretreated with 0 or 100 U/ml mouse IFN-β for 18 h and subsequently infected with
711 WT-MHV or ExoN(-) virus at an MOI of 1 PFU/cell. At 12 h post-infection, cell culture
712 supernatants were harvested for each virus and treatment group and the number of virion genome
713 RNA copies present (particles) in the supernatant was determined by one-step qRT-PCR. Using
714 the determined number of particles, an equivalent number of virus particles from each virus and

715 treatment group were mixed with an equal number of WT silent or ExoN(-) silent virus particles.
716 This mixture was then used to infect a fresh monolayer of untreated DBT cells. At 24 h post-
717 infection, cell culture supernatants were collected, RNA was extracted, and the number of virion
718 genome RNA copies for each original virus and treatment group relative to their respective silent
719 standard viruses was determined by one-step qRT-PCR and is reported as the change in fitness
720 relative to the silent virus standard. Error bars represent SEM (n=6). For each panel, statistical
721 significance compared to untreated WT-MHV or ExoN(-) infection, respectively, is denoted and
722 was determined by Student's *t* –test. *, $P < 0.05$, *** $P < 0.001$, n.s.= not significant.

FIGURE 1.

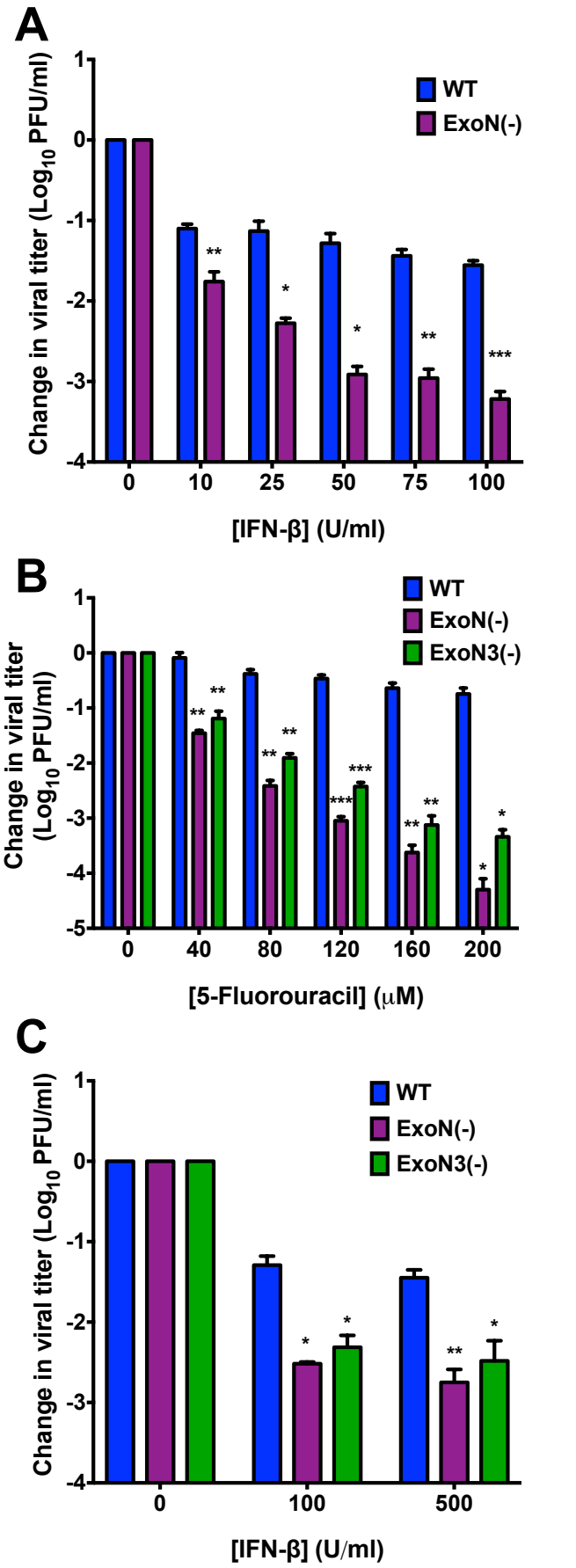
A
WT
ExoN(-)
Change in viral titer (Log10 PFU/ml)
1
0
-1
-2
-3
-4
**
*
*
**
***
0
10
25
50
75
100
[IFN-β] (U/ml)
B
WT
ExoN(-)
ExoN3(-)
Change in viral titer (Log10 PFU/ml)
1
0
-1
-2
-3
-4
-5
**
**
**
**
***
***
**
**
*
*
0
40
80
120
160
200
[5-Fluorouracil] (μM)
C
WT
ExoN(-)
ExoN3(-)
Change in viral titer (Log10 PFU/ml)
1
0
-1
-2
-3
-4
*
*
**
*
0
100
500
[IFN-β] (U/ml)

FIGURE 2.

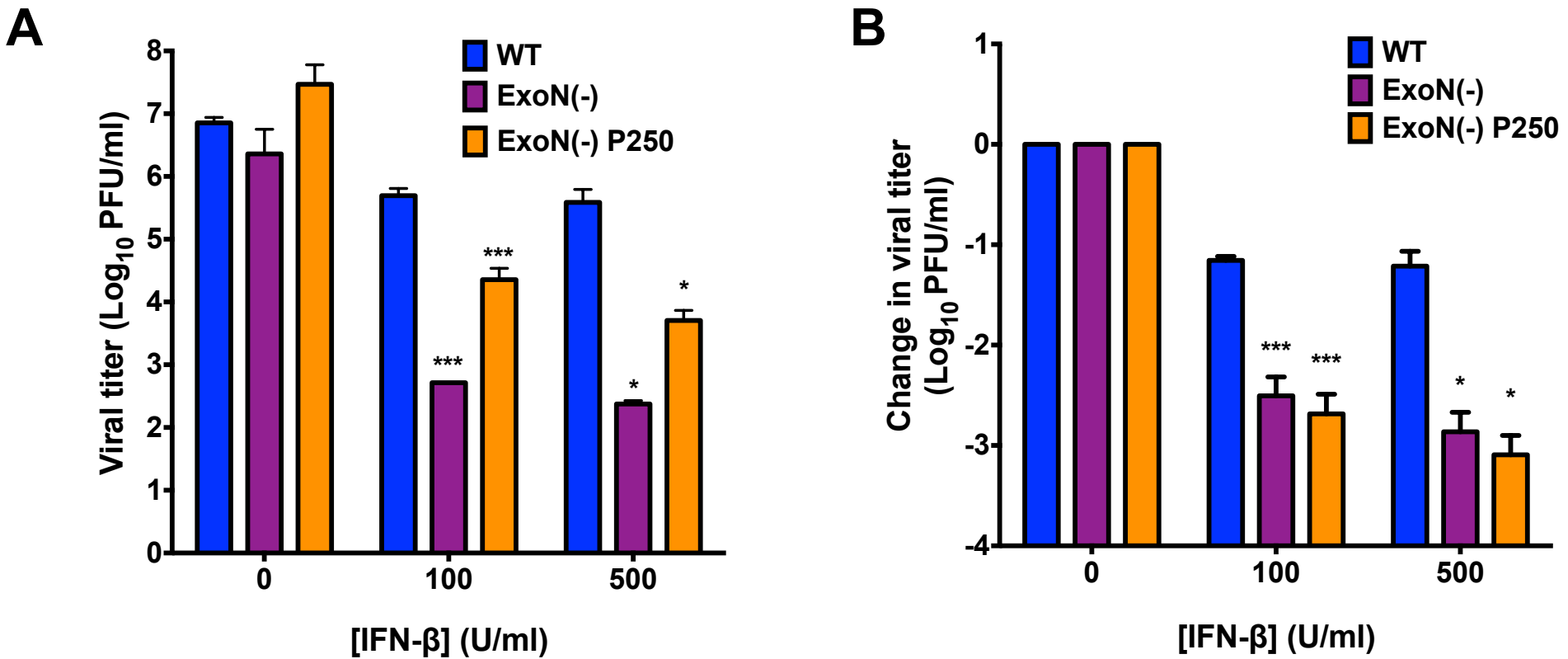
A
Viral titer (Log10 PFU/ml)
WT
ExoN(-)
ExoN(-) P250
***
***
*
*
0
100
500
[IFN-β] (U/ml)
B
Change in viral titer (Log10 PFU/ml)
WT
ExoN(-)
ExoN(-) P250
***
***
*
*
0
100
500
[IFN-β] (U/ml)

FIGURE 3.

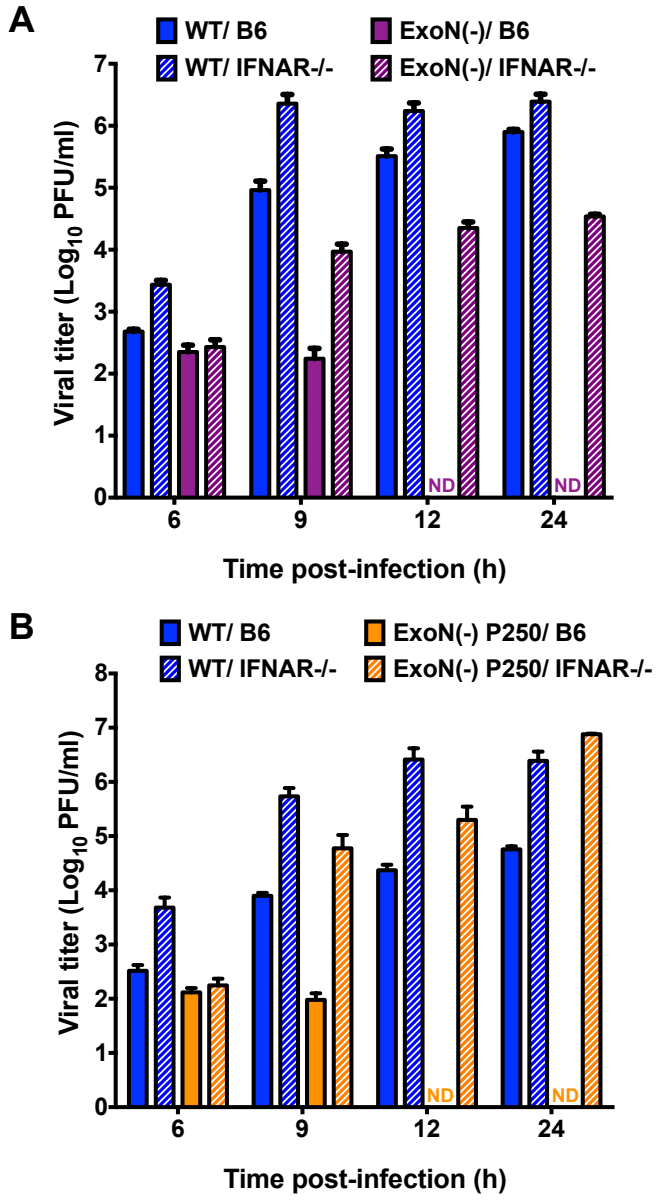
A
WT/ B6
ExoN(-)/ B6
WT/ IFNAR-/-
ExoN(-)/ IFNAR-/-
Viral titer (Log10 PFU/ml)
0
1
2
3
4
5
6
7
ND
ND
6
9
12
24
Time post-infection (h)
B
WT/ B6
ExoN(-) P250/ B6
WT/ IFNAR-/-
ExoN(-) P250/ IFNAR-/-
Viral titer (Log10 PFU/ml)
0
1
2
3
4
5
6
7
8
ND
ND
6
9
12
24
Time post-infection (h)

FIGURE 4.

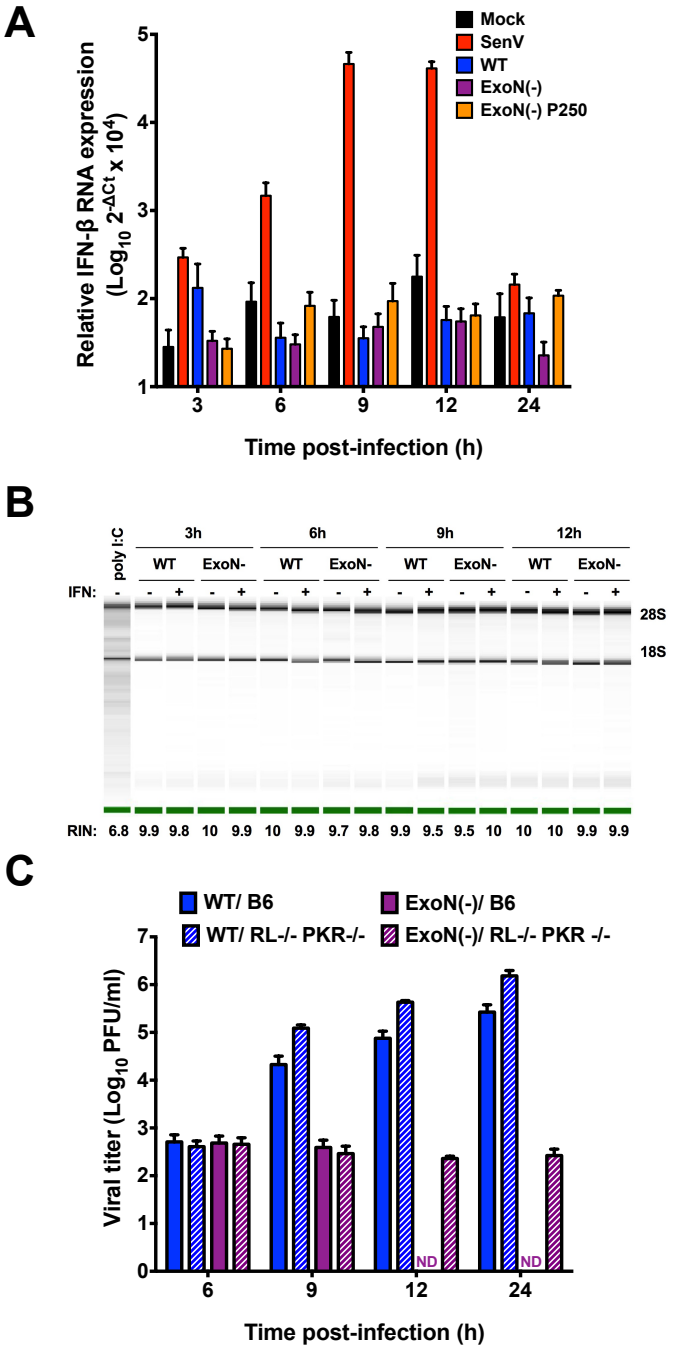
A
Mock
SenV
WT
ExoN(-)
ExoN(-) P250
Relative IFN-β RNA expression
(Log10 2-ΔCt x 10^4)
5
4
3
2
1
3
6
9
12
24
Time post-infection (h)
B
poly I:C
3h
6h
9h
12h
WT
ExoN-
IFN:
-
+
28S
18S
RIN:
6.8 9.9 9.8 10 9.9 10 9.9 9.7 9.8 9.9 9.5 9.5 10 10 10 9.9 9.9
C
WT/ B6
ExoN(-)/ B6
WT/ RL-/- PKR-/-
ExoN(-)/ RL-/- PKR -/-
Viral titer (Log10 PFU/ml)
7
6
5
4
3
2
1
0
ND
ND
6
9
12
24
Time post-infection (h)

FIGURE 5.

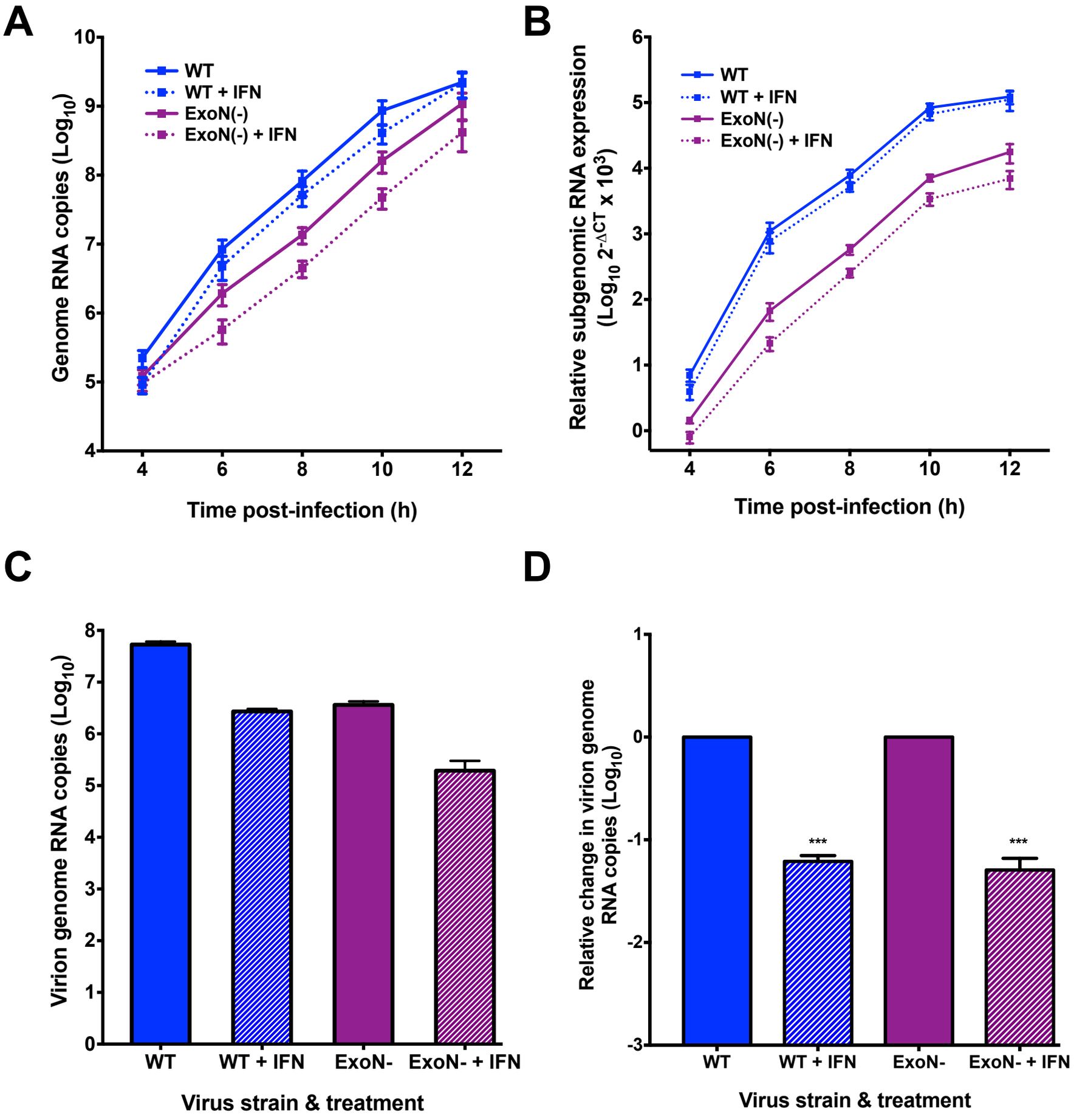
A
Genome RNA copies (Log10)
Time post-infection (h)
WT
WT + IFN
ExoN(-)
ExoN(-) + IFN
B
Relative subgenomic RNA expression (Log10 2-ΔCT x 10^3)
Time post-infection (h)
WT
WT + IFN
ExoN(-)
ExoN(-) + IFN
C
Virion genome RNA copies (Log10)
WT
WT + IFN
ExoN-
ExoN- + IFN
Virus strain & treatment
D
Relative change in virion genome RNA copies (Log10)
***
***
WT
WT + IFN
ExoN-
ExoN- + IFN
Virus strain & treatment

FIGURE 6.

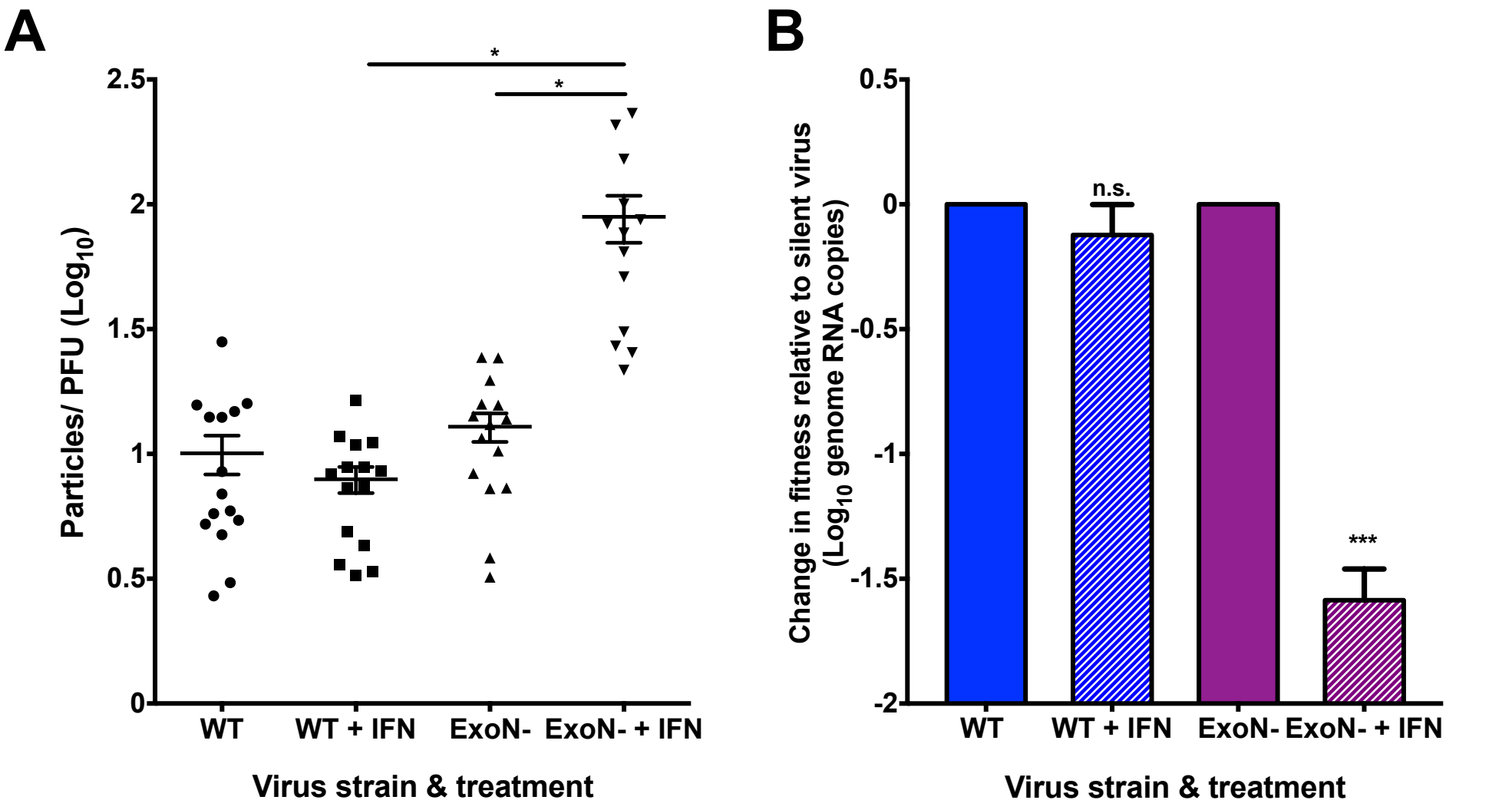
A
*
*
2.5
2
1.5
1
0.5
0
Particles/ PFU (Log10)
WT
WT + IFN
ExoN-
ExoN- + IFN
Virus strain & treatment
B
0.5
0
-0.5
-1
-1.5
-2
Change in fitness relative to silent virus (Log10 genome RNA copies)
n.s.
***
WT
WT + IFN
ExoN-
ExoN- + IFN
Virus strain & treatment